


Article

Ionic-Liquid Gating in Two-Dimensional TMDs: The Operation Principles and Spectroscopic Capabilities

Daniel Vaquero ¹, Vito Clericò ¹ , Juan Salvador-Sánchez ¹, Jorge Quereda ¹, Enrique Diez ^{1,*} and Ana M. Pérez-Muñoz ^{1,2,*}

¹ Nanotechnology Group, USAL–Nanolab, Universidad de Salamanca, E-37008 Salamanca, Spain; danivaqu@usal.es (D.V.); vito_clerico@usal.es (V.C.); juan2s@usal.es (J.S.-S.); J.Quereda@usal.es (J.Q.)

² FIW Consulting S.L., Gabriel Garcia Marquez, 4 las Rozas, E-28232 Madrid, Spain

* Correspondence: enrisa@usal.es (E.D.); anaperezmu@usal.es (A.M.P.-M.)

Abstract: Ionic-liquid gating (ILG) is able to enhance carrier densities well above the achievable values in traditional field-effect transistors (FETs), revealing it to be a promising technique for exploring the electronic phases of materials in extreme doping regimes. Due to their chemical stability, transition metal dichalcogenides (TMDs) are ideal candidates to produce ionic-liquid-gated FETs. Furthermore, as recently discovered, ILG can be used to obtain the band gap of two-dimensional semiconductors directly from the simple transfer characteristics. In this work, we present an overview of the operation principles of ionic liquid gating in TMD-based transistors, establishing the importance of the reference voltage to obtain hysteresis-free transfer characteristics, and hence, precisely determine the band gap. We produced ILG-based bilayer WSe₂ FETs and demonstrated their ambipolar behavior. We estimated the band gap directly from the transfer characteristics, demonstrating the potential of ILG as a spectroscopy technique.

Keywords: ionic liquid gating; ionic gate spectroscopy; ambipolar FETs; transition metal dichalcogenides



Citation: Vaquero, D.; Clericò, V.; Salvador-Sánchez, J.; Quereda, J.; Diez, E.; Pérez-Muñoz, A.M. Ionic-Liquid Gating in Two-Dimensional TMDs: The Operation Principles and Spectroscopic Capabilities. *Micromachines* **2021**, *12*, 1576. <https://doi.org/10.3390/mi12121576>

Academic Editors: Amalio Fernández-Pacheco and Javier Pablo-Navarro

Received: 15 November 2021

Accepted: 15 December 2021

Published: 17 December 2021

Publisher's Note: MDPI stays neutral with regard to jurisdictional claims in published maps and institutional affiliations.



Copyright: © 2021 by the authors. Licensee MDPI, Basel, Switzerland. This article is an open access article distributed under the terms and conditions of the Creative Commons Attribution (CC BY) license (<https://creativecommons.org/licenses/by/4.0/>).

1. Introduction

The discovery of two-dimensional materials unleashed a revolution in nanoelectronics during the last decade [1]. This family of materials holds enormous promise for the development of a new generation of semiconductor devices and, over the last few years, a considerable amount of effort has been invested in studying them and developing suitable devices that take advantage of their properties.

In 2011, Kis et al. demonstrated for the first time a field-effect transistor (FET) in which a bilayer MoS₂ crystal was used as the semiconductor channel [2]. Since then, similar devices have been developed using several different two dimensional (2D) materials, and the device geometry, materials, and fabrication methods have been greatly improved [3].

However, FETs have certain fundamental limitations that cannot be easily overcome: the dielectric breakdown of the insulating layer and the presence of charged impurities between the gate electrode and the 2D channel results in a limited gating capability, which is often not sufficient to reach ambipolar response in 2D semiconductor devices. The technique of ionic-liquid gating (ILG) aims to overcome these fundamental limitations by replacing the dielectric material in conventional FETs with ionic liquids [4] with movable charged ions [5–8]. In recent years, ILG-based 2D transistors have been tested by a number of research groups, allowing them to achieve extremely large accumulations of charge carriers, up to 5×10^{14} electrons/cm² while operating at moderate voltages within ± 3 V [9].

Ionic-gating experiments have been widely used to control and investigate the electronic properties of oxides [7,10], nitrides [11], organic semiconductors [12–14], carbon-related materials [15], and III–V semiconductor nanowires [16–19]. The extreme tunability of charge carrier concentrations that can be obtained by this technique has allowed the

attainment of new physical regimes, achieving, for example, superconductivity in band-insulating materials such as SrTiO₃ (STO) [20], ZrNCl [11], or KTaO₃ [21]. Currently, ILG has been established as a promising technique not only from an applied point of view, but also to obtain fundamental knowledge about the phase diagrams of novel materials [9,22]. More recently, ionic-gating experiments have moved forward through other inorganic systems, such as two-dimensional transition metal dichalcogenides (TMDs).

In this work, we present the operation principles for the use of ILG in TMD-based transistors. Due to their chemical stability, two-dimensional TMDs are ideal candidates to produce ionic liquid-gated FETs [23,24]. The very large geometrical capacitance of ionic liquid-gated devices allowed the observation of superconductivity in MoS₂ [25–31] and WS₂ [32–34], among other TMDs [35–37]. This technique has also enabled light emission by TMD-FETs operating in the ambipolar injection regime [38,39] and the enhancement of the electron–phonon interaction in multivalley TMDs [24,29,40]. Furthermore, as we present in this work, ILG-based TMD transistors grant the possibility of determining the band gap of semiconducting TMDs quantitatively from simple transport measurements [39,41–44].

2. Results

2.1. Device Fabrication and Geometry

Figure 1a schematically shows the geometry of a TMD-based ILG transistor. To illustrate the typical geometry and behavior of this family of transistors, we refer to the device shown in Figure 1b. In our case, the channel is a thin bilayer WSe₂ crystal, fabricated by standard mechanical exfoliation and ulterior transfer onto a SiO₂/Si substrate. The metallic electrodes were fabricated by e-beam lithography and evaporation of titanium and gold (5/45 nm). In addition to the four electrodes connected to the WSe₂ flake, two electrodes were fabricated to act as the gate (V_g) and reference (V_{ref}) electrodes. As a final step, the whole device was covered with a droplet of ionic liquid (DEME-TFSI), contacting the semiconductor channel, as well as the reference and gate electrodes (see Section S1 in Supplementary Materials for more information on the IL and its deposition). To minimize the exposure of the IL to the gold pads, the whole device was covered with polymethyl methacrylate (PMMA), leaving an exposed rectangular window on top of the semiconductor channel for placing the droplet (see Figure 1c).

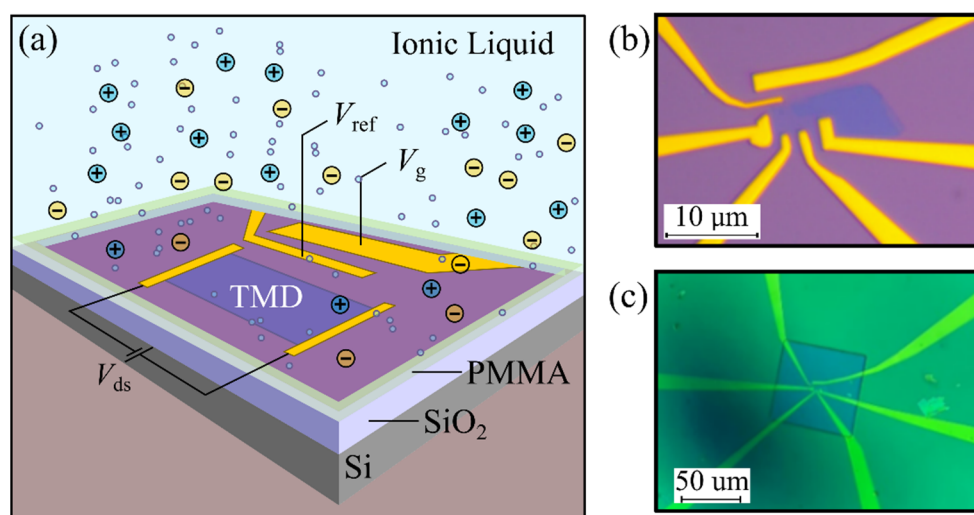


Figure 1. (a) Full schematics of an ionic-liquid-gated field-effect transistor (FET), showing the gate and reference electrodes, as well as the electrical circuit used to bias and measure the device. (b) Optical microscope image of a bilayer of WSe₂ contacted in Hall bar configuration (the scale bar is 10 μm). (c) Optical microscope image of the device's polymethyl methacrylate (PMMA) windows (the scale bar is 50 μm).

2.2. Basic Device Operation and Doping Mechanisms

The basic operation of the ILG transistor is depicted in Figure 2a,b. When a gate voltage is applied, the finite-sized ions accumulate in consecutive layers close to the TMD channel, forming a nanocapacitor that is typically 1 nm or less. It enhances a large electric field, resulting in a strong gating effect that can be controlled by the application of voltage to the gate electrode.

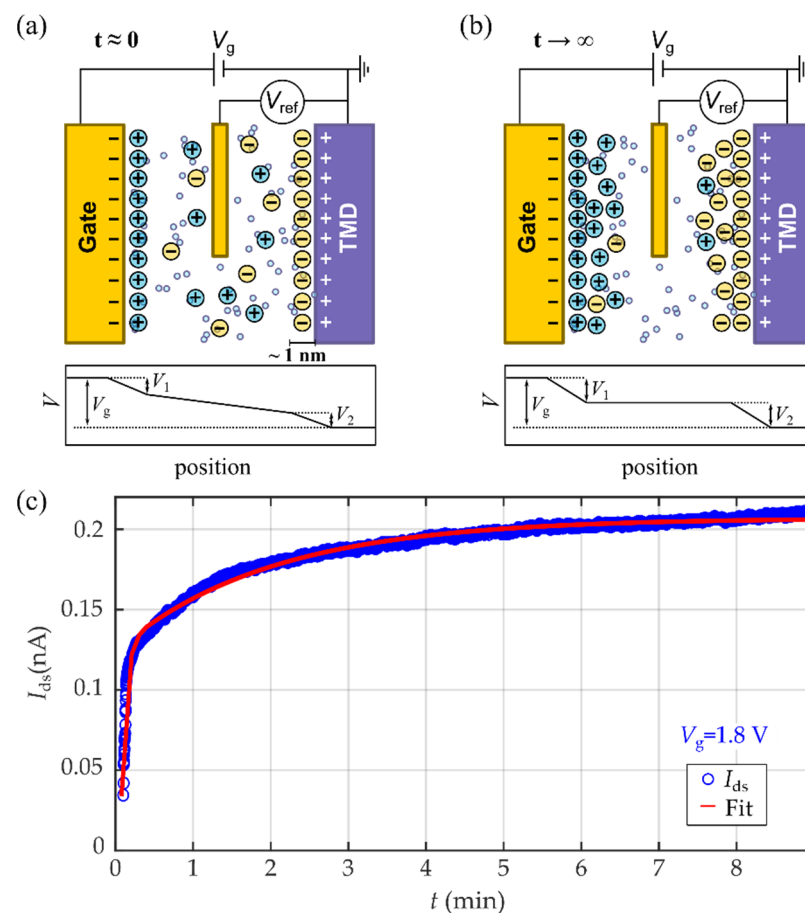


Figure 2. (a,b) Schematic diagram of the gating mechanism immediately after applying a gate voltage (a) and once the electric field inside the ionic liquid is fully screened (b). (c) Evolution of the drain source current (blue dots), measured immediately after switching V_g from 0 to 1.8 V. The current progressively increases as the Electrostatic Double Layer (EDL) is formed. The formation process of the EDL can be fitted to the charge process of two plane-parallel capacitors.

Figure 2c shows the time evolution of the drain-source current in the few-layer WSe_2 IL-gated transistor, measured while switching the gate voltage from 0 to 1.8 V. The measured current I_{ds} can be well-fitted to the equation for the charge process of two plane-parallel capacitors with different characteristic times:

$$I_{ds}(t) = A + B \left(1 - e^{-\frac{t}{\alpha_1}} \right) + C \left(1 - e^{-\frac{t}{\alpha_2}} \right) \quad (1)$$

where $\tau_{1,2} = \frac{1}{\alpha_{1,2}}$ are the characteristic times of the formation of the ionic layers that we use as fitting parameters. We obtained the characteristic times of $\tau_1 = 30$ s and $\tau_2 = 23$ min. These two characteristic times can be associated to the presence of two different charging processes. One is related to the fast formation of the first ion compact shells. The other one is caused by a slower migration and accumulation of ionic species in consecutive layers until the electric field inside the ionic liquid is fully screened [45].

While in early works, the doping effect in IL-gated FETs was attributed solely to the electrostatic screening of the accumulated charges at the interfaces, it is now clear that two main mechanisms govern ionic-liquid gating, depending on the characteristics of both the electrolyte and the material used as a channel [46]: electrostatic doping (described above) and electrochemical doping. For this second mechanism, the migration of ions within the material plays a key role and may induce an irreversible behavior caused by chemical degradation. Electrochemical doping is often the dominant gating mechanism when the IL is used in combination with transition metal oxides. In this case, the doping process also involves the migration of oxygen atoms from the crystallographic unit cell. The oxygen atoms act as dopants, enabling the introduction of charge carriers into the system [47–49]. However, in the case of semiconducting TMDs, ionic gating has an almost pure electrostatic effect and does not cause any chemical modification, as long as the applied gate voltage is kept within a suitable range, which results in stable and reversible transistor operation.

2.3. The Need for a Reference Electrode

In a conventional metal–oxide–semiconductor field-effect transistor (MOSFET), the applied gate voltage, V_g , uniformly drops across the gate dielectric. However, as depicted in Figure 2a,b and discussed above, in EDL transistors the voltage drop concentrates in the neighboring regions of the gate electrode (V_1) and the channel (V_2). Thus, in equilibrium we have:

$$V_g = V_1 + V_2, \quad (2)$$

and only a portion of V_2 of the applied voltage, V_g , contributes to gating.

In the hypothetical situation in which V_1 becomes negligible, the applied gate voltage, V_g , drops entirely at the IL/WSe₂ interface ($V_2 = \Delta V_g$). Experimentally, in ILG measurements, the gate electrode is usually (and intentionally) fabricated to have a large surface area, so the contribution of V_1 can be minimal; however, it cannot be neglected.

In general, V_1 and V_2 do not change linearly with V_g , and, furthermore, they may fluctuate over time and/or present hysteretic behaviors. In consequence, it is necessary to introduce a reference electrode, V_{ref} , to monitor V_2 situated in contact with the ionic liquid (see Figure 2a,b). For sufficiently long times, once the EDLs are fully formed, V_{ref} will be given by:

$$V_{ref} = V_g - V_1 = V_2. \quad (3)$$

Thus, V_{ref} provides us with a direct measurement of the voltage drop at the liquid/TMD interface, which is responsible for the gating effect.

2.4. Nonmonotonic Behavior in Transfer Characteristics and Estimation of Semiconductor Band Gap

Figure 3 shows the transfer characteristic of a WSe₂ ILG transistor, measured at 240 K (see Section S2 for measurements at other temperatures). As mentioned in the previous section, when the drain-source current is plotted against the gate voltage, V_G (Figure 3a), a large hysteresis appears because of the slow process of ion diffusion in the ionic liquid. However, this hysteresis largely decreases when I_{ds} is represented as a function of V_{ref} (Figure 3b).

The large shifts in the Fermi energy that can be achieved in ILG transistors allow us to observe ambipolar conduction in the transfer characteristic even while applying moderate gate voltages. A large source-drain current, I_{ds} , is measured for both high negative and positive V_g . When the Fermi level is in the WSe₂ band gap (OFF state), the measured current is just 10 pA, indicating there is almost no hopping conductivity because of intragap states or unintentional dopants in the material [41] and confirming the high quality of the WSe₂ flake.

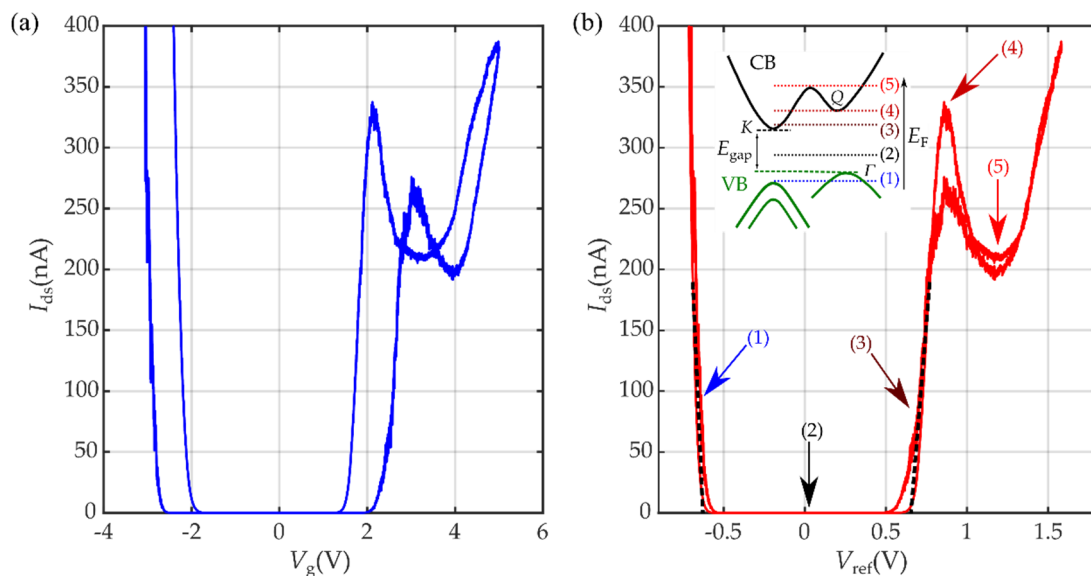


Figure 3. Transfer characteristic of a few-layer WSe₂ ionic-liquid-gated FET, measured at $V_{ds} = 0.1$ V as a function of (a) the gate voltage, V_g , (sweep rate at 1 mV/s) and (b) the reference voltage, V_{ref} . The threshold voltage values for electrons (V_{th}^e) and holes (V_{th}^h) were determined by linearly extrapolating to zero the I_{ds} - V_{ref} characteristics, as indicated by the black dashed lines. All measurements were taken at 240 K. The inset in Figure 2b depicts a schematic illustration of the conduction and valence band edges of bilayer WSe₂, showing the K and Q valleys in the conduction band, as well as the (spin-split) K valley and the Γ valley in the valence band. The conduction band edge consists of a single line because at the temperature of our experiments (240 K), spin-splitting is smaller than the thermal energy and it can be disregarded. E_{gap} indicates the energy distance between the conduction band edges at the K and Γ valleys. In the valence band in WSe₂, the high-spin-split K valley is lower than the Γ valley in terms of binding energy. Colored arrows and numbers depict the position of the Fermi energy at different V_{ref} in the transfer curve.

For positive gate voltages ($V_g > 0$), the transfer curve shows a nonmonotonic behavior, also described in the literature using different ionic liquids [50]. This has been found to be related to a nonlinearity that is present in the electron density because of intervalley scattering processes. This intervalley scattering becomes possible when the chemical potential is shifted into a higher energy valley. WSe₂ bilayers exhibit an indirect band gap between the conduction band minimum at Γ and the valence band maximum at K in the first Brillouin zone (BZ) [51]. Upon adding electrons, the K valley is filled first to above a certain value (denoted by (4) in the inset of Figure 3b), and the Q valley also starts to be filled. This inflection point enabled the quantitative determination of the energy difference between the K and Q valleys of monolayer WSe₂ in the literature, $E_Q - E_K = 108$ meV [50]. We estimated the energy difference between the K and Q valleys for bilayer WSe₂, $E_Q - E_K = 40$ meV (see Section S3), to be in agreement with the value obtained in the literature [51]. For negative gate voltages ($V_g < 0$), this nonmonotonic behavior is not observed. In this case, the second valley to be depleted of electrons would be the valley centered at K. However, the required hole density to reach this second valley is above the values achieved in our measurements.

2.5. ILG: A Spectroscopy Technique to Estimate the Semiconductor Band Gap

Currently, determining the band gap of two-dimensional semiconductors is usually undertaken using optical techniques [52–54] or by scanning tunneling spectroscopy (STS) [55,56], although complex techniques, such as angle-resolved photoemission spectroscopy (ARPES) [57,58], have also been used. However, these first two commonly used techniques require modeling of the measured data to extract a quantitative value for the gap. In optical techniques, an analysis of excited exciton states is required, this being a hard approach for indirect band gap semiconductors. In the case of the STS, the measured differ-

ential conductance must be modeled because the tip acts as a local gate, shifting the energy of the band edge and modifying the probability of electrons tunneling through vacuum.

As recently proved by Morpurgo et al. [53], IL gating can be used as a spectroscopy technique to precisely determine the band gap of a semiconductor from simple transport measurements. Because of the close proximity of the ionic liquid to the semiconductor channel, donor or acceptor impurities are negligible at the interface. Thus, a change in the gate voltage (or more precisely in the reference potential, ΔV_{ref}) is directly related to a shift in chemical potential, and the difference between V_{th}^e and V_{th}^h is a direct measurement of the semiconductor band gap.

A change in reference voltage induces a change in both the chemical potential, $\Delta\mu$, and the electrostatic potential, $\Delta\varphi$:

$$e\Delta V_{\text{ref}} = \Delta\mu + e\Delta\varphi. \quad (4)$$

The electrostatic potential in a parallel-plate capacitor can be defined as:

$$\Delta\varphi = \frac{e\Delta n}{C_G}, \quad (5)$$

where Δn is the density of accumulated charge carriers at the capacitor plate and C_G is the geometric capacitance.

For Fermi energies within the TMD band gap, Δn is small because, ideally, there are no available states to be occupied by charge carriers, and the term $\Delta\varphi$ in Equation (4) can be disregarded. In this situation, a shift in gate voltage induces an identical shift in chemical potential:

$$e\Delta V_{\text{ref}} = \Delta\mu. \quad (6)$$

Therefore, the band gap of the semiconductor channel, E_{gap} , can then be determined as:

$$E_{\text{gap}} = e \left(V_{\text{th}}^e - V_{\text{th}}^h \right), \quad (7)$$

since V_{th}^e and V_{th}^h correspond to having μ located, respectively, at the conduction and valence band edges.

Figure 4 shows the transfer characteristics of the WSe₂ device measured at different positive (Figure 4a) and negative (Figure 4b) drain-source voltages, V_{ds} . The threshold voltage values for electrons, V_{th}^e , and holes, V_{th}^h , were obtained by linearly extrapolating to zero the $I_{\text{ds}} - V_{\text{ref}}$ characteristics, (see black dashed lines in Figure 3b). To perform the extrapolation properly, it is important to identify a sufficiently large range of V_{ref} in the linear regime, out of the sub-threshold region, in which I_{ds} increases exponentially on V_{ref} [59].

The band gap is estimated by extrapolating to $V_{\text{ds}} = 0$ V. We obtain:

$$E_{\text{WSe}_2} = e \left(V_{\text{th}}^e - V_{\text{th}}^h \right) = 1.3 \text{ eV},$$

with an $\sim\pm 5\%$ experimental error that originated from the extrapolation procedure. This value agrees with the band gap measured with experimental techniques (1.5–1.6 eV) [51,59–62], as well as with the value estimated theoretically for bilayer WSe₂ (1.1 eV) [45]. At high V_{ds} , linear shifts in the threshold voltage appear. This threshold voltage was previously associated in WS₂ with uncertainties in the measurements [41] and here we relate it to the position dependence of the reference electrode, its geometry and area indicating the need to measure with low V_{ds} because of the strong dependence on the localization of the reference electrode. The leakage current was also measured during the experiment, keeping the values below 0.05 nA (see Section S4 for more information).

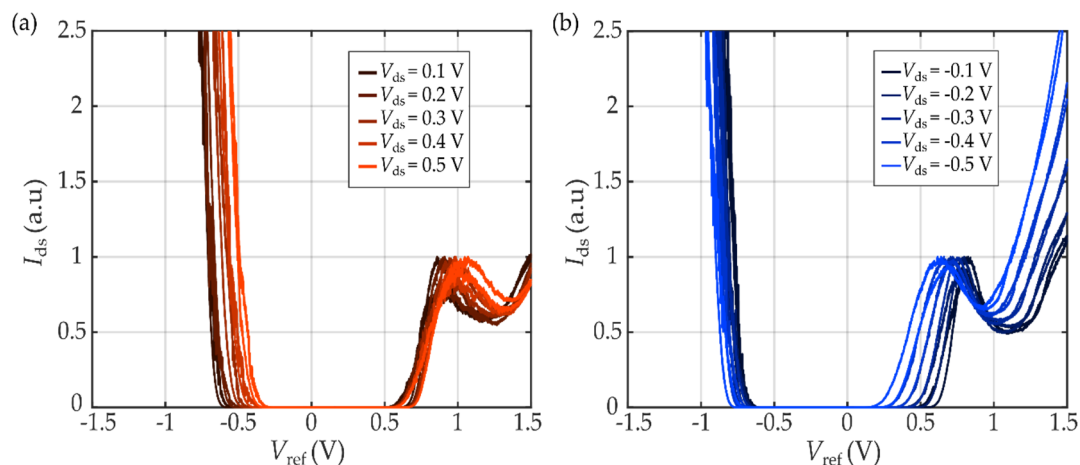


Figure 4. Drain current, I_{ds} , versus reference voltage, V_{ref} , at different (a) positive and (b) negative drain-source voltages, V_{ds} . The threshold voltage values were determined by linearly extrapolating to zero the $I_{ds} - V_{ref}$ characteristics and the WSe₂ energy band gap was estimated by extrapolating V_{ds} to zero.

3. Conclusions

In this work, we described and demonstrated the operation principles of ionic liquid gating in TMD-based transistors. We produced an ambipolar field-effect transistor with bilayer WSe₂ flake crystals, explaining the importance of the reference voltage, V_{ref} , for obtaining hysteresis-free transfer characteristics. ILG allowed us to obtain steep subthreshold slopes for both electrons and holes and extremely low OFF-state currents. We obtained evidence of the potential spectroscopic capabilities of ionic-liquid-gated transistors by acquiring the band gap of bilayer WSe₂ directly from those measurements.

The possibility of quantitatively determining the band gaps and band offsets directly from simple transfer characteristics makes the IL gating a promising new technique, ideal for characterizing 2D semiconductor materials and their heterostructures.

Supplementary Materials: Supplementary material is available online at <https://www.mdpi.com/article/10.3390/mi12121576/s1>, S1: Deposition of the ionic liquid DEME-TFSI, S2: Transfer curves at different temperatures, Figure S1: Transfer characteristics of the bilayer WSe₂ ionic liquid-gated transistor, S3: Estimation of the energy splitting between valleys Q-K in bilayer WSe₂, S4: Measuring the gate leakage current and the linear dependence of V_{ref} and V_{gate} , Figure S2 Gate leakage current, I_G , measured between the gate electrode and the device as function of the reference voltage, V_{ref} while sweeping the gate voltage, V_g , at 1 mV/s.

Author Contributions: E.D. and A.M.P.-M. conceived and supervised the research; V.C., J.S.-S. and A.M.P.-M. fabricated the devices; D.V., J.Q. and A.M.P.-M. carried out the experimental measurements and data analysis. The article was written with contributions from all the authors, coordinated by A.M.P.-M. All authors have read and agreed to the published version of the manuscript.

Funding: This research was funded by Agencia Estatal de Investigación of Spain (Grant PID2019-106820RB) and the Junta de Castilla y León (Grants SA256P18 and SA121P20), including funding by ERDF/FEDER. J.Q. acknowledges financial support from MICINN (Spain) through the Juan de la Cierva-Incorporación program. A.M.P.-M. acknowledges financial support from the Spanish Ministry of Science and Innovation under the Torres Quevedo grant, TQ2019-010689/AEI/10.13039/501100011033. D.V. acknowledges financial support from the Ministerio de Universidades (Spain) (Ph.D. contract FPU19/04224), including funding from ERDF/FEDER. J.S. acknowledges financial support for his Ph.D. contract from the Consejería de Educación, Junta de Castilla y León, and ERDF/FEDER.

Data Availability Statement: The data that support the findings of this study are available from the corresponding author upon reasonable request.

Acknowledgments: We thank Adrián Martín for his help during sample fabrication and the Research Group on High-Frequency Nanoelectronic Devices of USAL-NANOLAB for the use a low-temperature probe station during the experimental measurements.

Conflicts of Interest: The authors declare no conflict of interest.

References

1. Novoselov, K.S.; Mishchenko, A.; Carvalho, A.; Castro Neto, A.H. 2D Materials and van Der Waals Heterostructures. *Science* **2016**, *353*, aac9439. [[CrossRef](#)]
2. Radisavljevic, B.; Radenovic, A.; Brivio, J.; Giacometti, V.; Kis, A. Single-Layer MoS₂ Transistors. *Nat. Nano* **2011**, *6*, 147–150. [[CrossRef](#)]
3. Liu, Y.; Duan, X.; Shin, H.J.; Park, S.; Huang, Y.; Duan, X. Promises and Prospects of Two-Dimensional Transistors. *Nature* **2021**, *591*, 43–53. [[CrossRef](#)] [[PubMed](#)]
4. Brattain, B.W.H.; Garrett, C.G.B. Experiments on the Interface Between Germanium and an Electrolyte. *Bell Syst. Tech. J.* **1954**, *34*, 129–176. [[CrossRef](#)]
5. Shimotani, H.; Asanuma, H.; Takeya, J.; Iwasa, Y. Electrolyte-Gated Charge Accumulation in Organic Single Crystals. *Appl. Phys. Lett.* **2006**, *89*, 203501. [[CrossRef](#)]
6. Shimotani, H.; Asanuma, H.; Tsukazaki, A.; Ohtomo, A.; Kawasaki, M.; Iwasa, Y. Insulator-to-Metal Transition in ZnO by Electric Double Layer Gating. *Appl. Phys. Lett.* **2007**, *91*, 15–18. [[CrossRef](#)]
7. Yuan, H.; Shimotani, H.; Tsukazaki, A.; Ohtomo, A.; Kawasaki, M.; Iwasa, Y. High-Density Carrier Accumulation in ZnO Field-Effect Transistors Gated by Electric Double Layers of Ionic Liquids. *Adv. Funct. Mater.* **2009**, *19*, 1046–1053. [[CrossRef](#)]
8. Yuan, H.; Shimotani, H.; Tsukazaki, A.; Ohtomo, A. Hydrogenation-Induced Surface Polarity Recognition and Proton Memory Behavior at Protic-Ionic-Liquid/Oxide Electric-Double-Layer Interfaces. *J. Am. Chem. Soc.* **2010**, *132*, 6672–6678. [[CrossRef](#)]
9. Bisri, S.Z.; Shimizu, S.; Nakano, M.; Iwasa, Y. Endeavor of Iontronics: From Fundamentals to Applications of Ion-Controlled Electronics. *Adv. Mater.* **2017**, *29*, 1607054. [[CrossRef](#)]
10. Yamada, Y.; Ueno, K.; Fukumura, T.; Yuan, H.T.; Shimotani, H.; Iwasa, Y.; Gu, L.; Tsukimoto, S.; Ikuhara, Y.; Kawasaki, M. Electrically Induced Ferromagnetism at Room Temperature in Cobalt-Doped Titanium Dioxide. *Science* **2011**, *332*, 1065–1067. [[CrossRef](#)]
11. Ye, J.T.; Inoue, S.; Kobayashi, K.; Kasahara, Y.; Yuan, H.T.; Shimotani, H.; Iwasa, Y. Liquid-Gated Interface Superconductivity on an Atomically Flat Film. *Nat. Mater.* **2010**, *9*, 125–128. [[CrossRef](#)]
12. Kim, S.H.; Hong, K.; Xie, W.; Lee, K.H.; Zhang, S.; Lodge, T.P.; Frisbie, C.D. Electrolyte-Gated Transistors for Organic and Printed Electronics. *Adv. Mater.* **2013**, *25*, 1822–1846. [[CrossRef](#)] [[PubMed](#)]
13. Xia, B.Y.; Cho, J.H.; Lee, J.; Ruden, P.P.; Frisbie, C.D. Comparison of the Mobility–Carrier Density Relation in Polymer and Single-Crystal Organic Transistors Employing Vacuum and Liquid Gate Dielectrics. *Adv. Mater.* **2009**, *21*, 2174–2179. [[CrossRef](#)]
14. Leger, J.; Berggren, M.; Carter, S.; Berggren, M.; Carter, S. *Iontronics: Ionic Carriers in Organic Electronic Materials and Devices*; CRC Press: Boca Raton, FL, USA, 2016.
15. You, A.; Be, M.A.Y.; In, I. Electrochemical Carbon Nanotube Field-Effect Transistor. *Appl. Phys. Lett.* **2007**, *78*, 1291. [[CrossRef](#)]
16. Lieb, J.; Demontis, V.; Prete, D.; Ercolani, D.; Zannier, V.; Sorba, L.; Ono, S.; Beltram, F.; Sacépé, B.; Rossella, F. Ionic-Liquid Gating of InAs Nanowire-Based Field-Effect Transistors. *Adv. Funct. Mater.* **2019**, *29*, 1804378. [[CrossRef](#)]
17. Demontis, V.; Zannier, V.; Sorba, L.; Rossella, F. Surface Nano-Patterning for the Bottom-Up Growth of III-V Semiconductor Nanowire Ordered Arrays. *Nanomaterials* **2021**, *11*, 2079. [[CrossRef](#)]
18. Ullah, A.R.; Carrad, D.J.; Krogstrup, P.; Nygård, J.; Micolich, A.P. Near-Thermal Limit Gating in Heavily Doped III-V Semiconductor Nanowires Using Polymer Electrolytes. *Phys. Rev. Mater.* **2018**, *2*, 25601. [[CrossRef](#)]
19. Carrad, D.J.; Mostert, A.B.; Ullah, A.R.; Burke, A.M.; Joyce, H.J.; Tan, H.H.; Jagadish, C.; Krogstrup, P.; Nygård, J.; Meredith, P. Hybrid Nanowire Ion-to-Electron Transducers for Integrated Bioelectronic Circuitry. *Nano Lett.* **2017**, *17*, 827–833. [[CrossRef](#)]
20. Ueno, K.; Nakamura, S.; Shimotani, H.; Ohtomo, A.; Kimura, N.; Nojima, T.; Aoki, H.; Iwasa, Y.; Kawasaki, M. Electric-Field-Induced Superconductivity in an Insulator. *Nat. Mater.* **2008**, *7*, 855–858. [[CrossRef](#)]
21. Ueno, K.; Nakamura, S.; Shimotani, H.; Yuan, H.T.; Kimura, N.; Nojima, T.; Aoki, H.; Iwasa, Y.; Kawasaki, M. Discovery of Superconductivity in KTaO₃ by Electrostatic Carrier Doping. *Nat. Nanotechnol.* **2011**, *6*, 408–412. [[CrossRef](#)] [[PubMed](#)]
22. Fujimoto, T.; Awaga, K. Electric-Double-Layer Field-Effect Transistors with Ionic Liquids. *Phys. Chem. Chem. Phys.* **2013**, *15*, 8983–9006. [[CrossRef](#)] [[PubMed](#)]
23. Yuan, H.T.; Toh, M.; Morimoto, K.; Tan, W.; Wei, F.; Shimotani, H.; Kloc, C.; Iwasa, Y. Liquid-Gated Electric-Double-Layer Transistor on Layered Metal Dichalcogenide, SnS₂. *Appl. Phys. Lett.* **2011**, *98*, 012102. [[CrossRef](#)]
24. Zhang, Y.; Ye, J.; Matsushashi, Y.; Iwasa, Y. Ambipolar MoS₂ Thin Flake Transistors. *Nano Lett.* **2012**, *12*, 1136–1140. [[CrossRef](#)]
25. Ye, J.T.; Zhang, Y.J.; Akashi, R.; Bahramy, M.S.; Arita, R.; Iwasa, Y. Superconducting Dome in a Gate-Tuned Band Insulator. *Science* **2012**, *338*, 1193–1196. [[CrossRef](#)] [[PubMed](#)]
26. Biscaras, J.; Chen, Z.; Paradisi, A.; Shukla, A. Onset of Two-Dimensional Superconductivity in Space Charge Doped Few-Layer Molybdenum Disulfide. *Nat. Commun.* **2015**, *6*, 8826. [[CrossRef](#)]
27. Costanzo, D.; Jo, S.; Berger, H.; Morpurgo, A.F. Gate-Induced Superconductivity in Atomically Thin MoS₂ Crystals. *Nat. Nanotechnol.* **2016**, *11*, 339–344. [[CrossRef](#)]

28. Costanzo, D.; Zhang, H.; Reddy, B.A.; Berger, H.; Morpurgo, A.F. Tunnelling Spectroscopy of Gate-Induced Superconductivity in MoS₂. *Nat. Nanotechnol.* **2018**, *13*, 483–488. [[CrossRef](#)]
29. Piatti, E.; De Fazio, D.; Daghero, D.; Tamalampudi, S.R.; Yoon, D.; Ferrari, A.C.; Gonnelli, R.S. Multi-Valley Superconductivity in Ion-Gated MoS₂ Layers. *Nano Lett.* **2018**, *18*, 4821–4830. [[CrossRef](#)]
30. Lu, J.M.; Zheliuk, O.; Leermakers, I.; Yuan, N.F.Q.; Zeitler, U.; Law, K.T.; Ye, J.T. Evidence for Two-Dimensional Ising Superconductivity in Gated MoS₂. *Science* **2015**, *350*, 1353–1358. [[CrossRef](#)]
31. Saito, Y.; Nakamura, Y.; Bahramy, M.S.; Kohama, Y.; Ye, J.; Kasahara, Y.; Nakagawa, Y.; Onga, M.; Tokunaga, M.; Nojima, T.; et al. Superconductivity Protected by Spin-Valley Locking in Ion-Gated MoS₂. *Nat. Phys.* **2016**, *12*, 144–149. [[CrossRef](#)]
32. Dhoot, A.S.; Israel, C.; Moya, X.; Mathur, N.D.; Friend, R.H. Large Electric Field Effect in Electrolyte-Gated Manganites. *Phys. Rev. Lett.* **2009**, *102*, 136402. [[CrossRef](#)]
33. Jo, S.; Costanzo, D.; Berger, H.; Morpurgo, A.F. Electrostatically Induced Superconductivity at the Surface of WS₂. *Nano Lett.* **2015**, *15*, 1197–1202. [[CrossRef](#)] [[PubMed](#)]
34. Lu, J.; Zheliuk, O.; Chen, Q.; Leermakers, I.; Hussey, N.E.; Zeitler, U.; Ye, J. Full Superconducting Dome of Strong Ising Protection in Gated Monolayer WS₂. *Proc. Natl. Acad. Sci. USA* **2018**, *115*, 3551–3556. [[CrossRef](#)] [[PubMed](#)]
35. Shi, W.; Ye, J.; Zhang, Y.; Suzuki, R.; Yoshida, M.; Miyazaki, J.; Inoue, N.; Saito, Y.; Iwasa, Y. Superconductivity Series in Transition Metal Dichalcogenides by Ionic Gating. *Sci. Rep.* **2015**, *5*, 12534. [[CrossRef](#)] [[PubMed](#)]
36. Kouno, S.; Sato, Y.; Katayama, Y.; Ichinose, A.; Asami, D. Superconductivity at 38 K at an Electrochemical Interface between Various Substrates. *Sci. Rep.* **2018**, *8*, 14731. [[CrossRef](#)]
37. Zeng, J.; Liu, E.; Fu, Y.; Chen, Z.; Pan, C.; Wang, C.; Wang, M.; Wang, Y.; Xu, K.; Cai, S.; et al. Gate-Induced Interfacial Superconductivity in 1T-SnSe₂. *Nano Lett.* **2018**, *18*, 1410–1415. [[CrossRef](#)]
38. Zhang, Y.J.; Oka, T.; Suzuki, R.; Ye, J.T.; Iwasa, Y. Electrically Switchable Chiral Light-Emitting Transistor. *Science* **2014**, *344*, 725–728. [[CrossRef](#)]
39. Jo, S.; Ubrig, N.; Berger, H.; Kuzmenko, A.B.; Morpurgo, A.F. Mono- and Bilayer WS₂ Light-Emitting Transistors. *Nano Lett.* **2014**, *14*, 2019–2025. [[CrossRef](#)]
40. Sohler, T.; Ponomarev, E.; Gibertini, M.; Berger, H.; Marzari, N.; Ubrig, N.; Morpurgo, A.F. Enhanced Electron-Phonon Interaction in Multivalley Materials. *Phys. Rev. X* **2019**, *9*, 31019. [[CrossRef](#)]
41. Braga, D.; Gutiérrez Lezama, I.; Berger, H.; Morpurgo, A.F. Quantitative Determination of the Band Gap of WS₂ with Ambipolar Ionic Liquid-Gated Transistors. *Nano Lett.* **2012**, *12*, 5218–5223. [[CrossRef](#)]
42. Lezama, I.G.; Ubaldini, A.; Longobardi, M.; Giannini, E.; Renner, C.; Kuzmenko, A.B.; Morpurgo, A.F. Surface Transport and Band Gap Structure of Exfoliated. *2D Mater.* **2014**, *1*, 021002. [[CrossRef](#)]
43. Berger, H.; Ponomarev, E.; Ubrig, N.; Gutie, I.; Morpurgo, A.F. Semiconducting van Der Waals Interfaces as Artificial Semiconductors. *Nano Lett.* **2018**, *18*, 5146–5152. [[CrossRef](#)]
44. Waelchli, A.; Scarfato, A.; Ubrig, N.; Renner, C.; Morpurgo, A.F. Hole Transport in Exfoliated Monolayer MoS₂. *ACS Nano* **2018**, *12*, 2669–2676. [[CrossRef](#)]
45. Oldham, K.B. A Gouy-Chapman-Stern Model of the Double Layer at a (Metal)/(Ionic Liquid) Interface. *J. Electroanal. Chem.* **2008**, *613*, 131–138. [[CrossRef](#)]
46. Lee, J.; Kaake, L.G.; Cho, J.H.; Zhu, X.; Lodge, T.P.; Frisbie, C.D. Ion Gel-Gated Polymer Thin-Film Transistors: Operating Mechanism and Characterization of Gate Dielectric Capacitance, Switching Speed, and Stability. *J. Phys. Chem. C* **2009**, *113*, 8972–8981. [[CrossRef](#)]
47. Li, M.; Han, W.; Jiang, X.; Jeong, J.; Samant, M.G.; Parkin, S.S.P. Suppression of Ionic Liquid Gate-Induced Metallization of SrTiO₃(001) by Oxygen. *Nano Lett.* **2013**, *13*, 4675–4678. [[CrossRef](#)] [[PubMed](#)]
48. Jeong, J.; Aetukuri, N.; Graf, T.; Schladt, T.D.; Samant, M.G.; Parkin, S.S.P. Suppression of Metal-Insulator Transition in VO₂ by Electric Field-Induced Oxygen Vacancy Formation. *Science* **2013**, *339*, 1402–1405. [[CrossRef](#)] [[PubMed](#)]
49. Perez-Muñoz, A.M.; Schio, P.; Poloni, R.; Fernandez-Martinez, A.; Rivera-Calzada, A.; Cezar, J.C.; Salas-Colera, E.; Castro, G.R.; Kinney, J.; Leon, C.; et al. In Operando Evidence of Deoxygenation in Ionic Liquid Gating of YBa₂Cu₃O_{7-x}. *Proc. Natl. Acad. Sci. USA* **2017**, *114*, 215–220. [[CrossRef](#)]
50. Zhang, H.; Berthod, C.; Berger, H.; Giamarchi, T.; Morpurgo, A.F. Band Filling and Cross Quantum Capacitance in Ion-Gated Semiconducting Transition Metal Dichalcogenide Monolayers. *Nano Lett.* **2019**, *19*, 8836–8845. [[CrossRef](#)]
51. Zhao, W.; Ribeiro, R.M.; Toh, M.; Carvalho, A.; Kloc, C.; Castro Neto, A.H.; Eda, G. Origin of Indirect Optical Transitions in Few-Layer MoS₂, WS₂, and WSe₂. *Nano Lett.* **2013**, *13*, 5627–5634. [[CrossRef](#)]
52. Poellmann, C.; Steinleitner, P.; Leierseder, U.; Nagler, P.; Plechinger, G.; Porer, M.; Bratschitsch, R.; Schüller, C.; Korn, T.; Huber, R. Resonant Internal Quantum Transitions and Femtosecond Radiative Decay of Excitons in Monolayer WSe₂. *Nat. Mater.* **2015**, *14*, 889–893. [[CrossRef](#)]
53. Hill, H.M.; Rigosi, A.F.; Roquelet, C.; Chernikov, A.; Berkelbach, T.C.; Reichman, D.R.; Hybertsen, M.S.; Brus, L.E.; Heinz, T.F. Observation of Excitonic Rydberg States in Monolayer MoS₂ and WS₂ by Photoluminescence Excitation Spectroscopy. *Nano Lett.* **2015**, *15*, 2992–2997. [[CrossRef](#)] [[PubMed](#)]
54. Raja, A.; Chaves, A.; Yu, J.; Arefe, G.; Hill, H.M.; Rigosi, A.F.; Berkelbach, T.C.; Nagler, P.; Schüller, C.; Korn, T.; et al. Coulomb Engineering of the Bandgap and Excitons in Two-Dimensional Materials. *Nat. Commun.* **2017**, *8*, 15251. [[CrossRef](#)]

55. Zhang, C.; Johnson, A.; Hsu, C.L.; Li, L.J.; Shih, C.K. Direct Imaging of Band Profile in Single Layer MoS₂ on Graphite: Quasiparticle Energy Gap, Metallic Edge States, and Edge Band Bending. *Nano Lett.* **2014**, *14*, 2443–2447. [[CrossRef](#)] [[PubMed](#)]
56. Chiu, M.H.; Zhang, C.; Shiu, H.W.; Chuu, C.P.; Chen, C.H.; Chang, C.Y.S.; Chen, C.H.; Chou, M.Y.; Shih, C.K.; Li, L.J. Determination of Band Alignment in the Single-Layer MoS₂ WSe₂ Heterojunction. *Nat. Commun.* **2015**, *6*, 7666. [[CrossRef](#)]
57. Cucchi, I.; Gutiérrez-Lezama, I.; Cappelli, E.; Walker, S.M.K.; Bruno, F.Y.; Tenasini, G.; Wang, L.; Ubrig, N.; Barreteau, C.; Giannini, E.; et al. Microfocus Laser-Angle-Resolved Photoemission on Encapsulated Mono-, Bi-, and Few-Layer 1T'-WTe₂. *Nano Lett.* **2019**, *19*, 554–560. [[CrossRef](#)]
58. Hamer, M.J.; Zultak, J.; Tyurnina, A.V.; Zólyomi, V.; Terry, D.; Barinov, A.; Garner, A.; Donoghue, J.; Rooney, A.P.; Kandyba, V.; et al. Indirect to Direct Gap Crossover in Two-Dimensional InSe Revealed by Angle-Resolved Photoemission Spectroscopy. *ACS Nano* **2019**, *13*, 2136–2142. [[CrossRef](#)]
59. Gutiérrez-Lezama, I.; Ubrig, N.; Ponomarev, E.; Morpurgo, A.F. Ionic Gate Spectroscopy of 2D Semiconductors. *Nat. Rev. Phys.* **2021**, *3*, 508–519. [[CrossRef](#)]
60. Desai, S.B.; Seol, G.; Kang, J.S.; Fang, H.; Battaglia, C.; Kapadia, R.; Ager, J.W.; Guo, J.; Javey, A. Strain-Induced Indirect to Direct Bandgap Transition in Multilayer WSe₂. *Nano Lett.* **2014**, *14*, 4592–4597. [[CrossRef](#)]
61. Tang, N.; Du, C.; Wang, Q.; Xu, H. Strain Engineering in Bilayer WSe₂ over a Large Strain Range. *Microelectron. Eng.* **2020**, *223*, 111202. [[CrossRef](#)]
62. Kumar, S.; Kaczmarczyk, A.; Gerardot, B.D. Strain-Induced Spatial and Spectral Isolation of Quantum Emitters in Mono- and Bilayer WSe₂. *Nano Lett.* **2015**, *15*, 7567–7573. [[CrossRef](#)] [[PubMed](#)]